Received: 7 January 2017 | Revised: 23 March 2017 | Accepted: 23 March 2017

DOI: 10.1002/col.22131

RESEARCH ARTICLE

WILEY

Comprehensive color solutions: CAM16, CAT16, and CAM16-UCS

Changjun Li[1,2] | Zhiqiang Li[1] | Zhifeng Wang[1] | Yang Xu[1] | Ming Ronnier Luo[3,4] | Guihua Cui[2] | Manuel Melgosa[5] | Michael H. Brill[6] | Michael Pointer[3]

[1] School of Electronics and Information Engineering, University of Science and Technology Liaoning, Anshan 114051, China

[2] Wenzhou University, 325035, China

[3] School of Design, University of Leeds, LS2 9JT, UK

[4] State Key Laboratory of Modern Optical Instrumentation, Zhejiang University, Hangzhou, China

[5] Department of Optics, University of Granada, 18071, Spain

[6] Datacolor, Lawrenceville, New Jersey 08648, USA

Correspondence
Ming Ronnier Luo, Colour Science, University of Leeds, Leeds, North Yorkshire LS2 9JT, United Kingdom.
Email: m.r.luo@leeds.ac.uk

Funding information
National Natural Science Foundation of China, Grant/Award Numbers: 61178053, 61575090, and 61475142; Ministry of Economy and Competitiveness of Spain (Research project FIS2016-80983-P) with contribution of European Regional Development Fund (ERDF); The Natural Science Foundation of Liaoning Province, China, Grant/Award Number: 2013020005

Abstract

The CIECAM02 color-appearance model enjoys popularity in scientific research and industrial applications since it was recommended by the CIE in 2002. However, it has been found that computational failures can occur in certain cases such as during the image processing of cross-media color reproduction applications. Some proposals have been developed to repair the CIECAM02 model. However, all the proposals developed have the same structure as the original CIECAM02 model and solve the problems concerned at the expense of losing accuracy of predicted visual data compared with the original model. In this article, the structure of the CIECAM02 model is changed and the color and luminance adaptations to the illuminant are completed in the same space rather than in two different spaces, as in the original CIECAM02 model. It has been found that the new model (named CAM16) not only overcomes the previous problems, but also the performance in predicting the visual results is as good as if not better than that of the original CIECAM02 model. Furthermore the new CAM16 model is simpler than the original CIECAM02 model. In addition, if considering only chromatic adaptation, a new transformation, CAT16, is proposed to replace the previous CAT02 transformation. Finally, the new CAM16-UCS uniform color space is proposed to replace the previous CAM02-UCS space. A new complete solution for color-appearance prediction and color-difference evaluation can now be offered.

KEYWORDS

chromatic adaptation, color-appearance models, color-difference evaluation CIECAM02, CAT02, CAM02-UCS, corresponding color datasets, LUTCHI color-appearance datasets

1 | INTRODUCTION

Ever since the recommendation of the CIECAM02 color-appearance model by CIE TC 8-01 "Color appearance modeling for color management systems," it has been used to predict color appearance under a wide range of viewing conditions,[1–3] to specify color appearance in terms of perceptual attributes,[4,5] to quantify color differences,[6] to propose a uniform color space (UCS),[7] and to provide a profile connection space for color management.[8–10] Some problems, however, were found with the CIECAM02 model. For example, computational failures can occur with applications in cross-media color image reproduction. In fact, this problem mainly comes from the lightness computation:

$$J = 100(A/A_w)^{cz}. \quad (1)$$

At this stage, we want to make it clear that all symbols used in this article have the same meaning as in the original CIE document.[1] Li and Luo[11] showed that A_w is positive for all CIE illuminants. However, the achromatic signal A, having the expression

$$A = \left[2R'_a + G'_a + (1/20)B'_a - 0.305\right] N_{bb} \quad (2)$$

can be negative. Thus, raising the negative ratio in the bracket of Equation 1 to the noninteger power cz, is not then possible, which causes early termination of the computing process.

The postadaptation cone signals R'_a, G'_a, and B'_a are obtained from the input tristimulus values X, Y, and Z via the illuminant color and luminance adaptations, which are defined as follows:

1.1 | Illuminant color adaptation

Firstly, the input X, Y, and Z values are transformed to a "sharp" sensor space, where the sensor response signals R, G, *and* B are given by:

$$\begin{pmatrix} R \\ G \\ B \end{pmatrix} = \mathbf{M}_{02} \begin{pmatrix} X \\ Y \\ Z \end{pmatrix} \quad (3)$$

Here, the matrix $\mathbf{M}_{02}$ is the built-in CAT02 matrix.[1–3,12] The color adaptation is then completed using the transform:

$$\begin{pmatrix} R_c \\ G_c \\ B_c \end{pmatrix} = \mathbf{\Lambda}(D) \begin{pmatrix} R \\ G \\ B \end{pmatrix} \quad (4)$$

where the matrix $\mathbf{\Lambda}(D)$ is the adaptation diagonal matrix:

$$\mathbf{\Lambda}(D) = \begin{pmatrix} D\frac{Y_w}{R_w} + 1 - D & & \\ & D\frac{Y_w}{G_w} + 1 - D & \\ & & D\frac{Y_w}{B_w} + 1 - D \end{pmatrix}. \quad (5)$$

To complete the luminance adaptation, the adapted color signals R_c, G_c, and B_c are transformed back to X, Y, and Z space via the inverse transform:

$$\begin{pmatrix} X_c \\ Y_c \\ Z_c \end{pmatrix} = \mathbf{M}_{02}^{-1} \begin{pmatrix} R_c \\ G_c \\ B_c \end{pmatrix}. \quad (6)$$

1.2 | Illuminant luminance adaptation

The X_C, Y_C, and Z_C tristimulus values of the corresponding color given by Equation 6 are transformed to the Hunt-Pointer-Estevez (HPE) cone space[13,14] for final luminance adaptation using the HPE matrix $\mathbf{M}_{HPE}$.[1–3] The HPE cone response signals R', G', and B' are given by the transformation:

$$\begin{pmatrix} R' \\ G' \\ B' \end{pmatrix} = \mathbf{M}_{HPE} \begin{pmatrix} X_c \\ Y_c \\ Z_c \end{pmatrix}. \quad (7)$$

Finally, the luminance adaptation is completed via a nonlinear transform[15]:

$$R'_a = \frac{\text{sign}(R') \quad 400(F_L|R'|/100)^{0.42}}{27.13 + (F_L|R'|/100)^{0.42}} + 0.1. \quad (8)$$

for the red channel, with corresponding equations for the green and blue channels.

Note that the derivative of the function defined by Equation 8 approaches infinity as R' approaches zero, resulting in unstable behaviour in this area. Various approaches[16,17] have been made to replace Equation 8. This article however, does not address this problem and Equation 8 is still used.

Note that Equations 3–6 are normally called the CAT02 transform and its full forward and inverse models have been given in previous literature.[18]

It is clear that the negative value of the achromatic signal A (Equation 2) comes from the two adaptation processes, and hence they were considered as the sources of the CIECAM02 problem. It is clear from Equations 2–8, that A is nonnegative if the HPE cone response signals R', G', and B' satisfy:

$$\begin{pmatrix} R' \\ G' \\ B' \end{pmatrix} = \mathbf{M}_{HPE}\mathbf{M}^{-1}\mathbf{\Lambda}(D)\mathbf{M} \begin{pmatrix} X \\ Y \\ Z \end{pmatrix} \geq 0. \quad (9)$$

Several approaches have been made to change the CAT02 matrix $\mathbf{M}$ so that the inequality (9) is satisfied. With the new matrix $\mathbf{M}$ in Equation 9, we have a corresponding new color appearance model and new chromatic adaptation transform (CAT). Li et al.[19] has pointed that if the matrix $\mathbf{M}$ equals the matrix $\mathbf{M}_{HPE}$, the inequality in Equation 9 holds for all colors with chromaticity coordinates located inside the domain (named as Ω_{CIE}) enclosed by the CIE spectrum locus and the purple line. In addition, Li et al.[20] defined another matrix. named as M_{CAM}, under the conditions: (a) the $\mathbf{M}_{CAM}$ matrix satisfies the inequality in Equation 9; and (b) with the $\mathbf{M}_{CAM}$ matrix the new CAM and new CAT fit the color appearance datasets[21–27] and corresponding color

datasets[21,28–33] as closely as possible. The accuracy of the predictions of the visual results using the $\mathbf{M}_{HPE}$ and $\mathbf{M}_{CAM}$ matrices, however, became worse compared with that obtained using the original CIECAM02 and CAT02 models.[20]

Brill and Süsstrunk[34–36] also found that the CIECAM02 model exhibited the so-called "yellow-blue problem" and the "purple problem," and they devised a rule for correcting them, which they called the nesting rule. If we let Ω_M be the chromaticity domain of all *X*, *Y*, and *Z* values giving non-negative *R*, *G*, *and B* response signals with the transformation defined by the matrix **M** (see Equation 3), and similarly for Ω_{HPE}, then the nesting rule can be exactly stated as[37]:

$$\Omega_{CIE} \subseteq \Omega_M \subseteq \Omega_{HPE}. \tag{10}$$

Brill and Süsstrunk reported that, with the original CAT02 matrix, the above nesting rule is not satisfied, which is the source of the CIECAM02 yellow-blue, and purple, problems. They gave a partial solution by solving the yellow-blue problem, but could not solve the purple problem. Recently, Li et al.[38] found that there were many matrices **M** that satisfied the nesting rule, and a special case was the matrix **M** being equal to the HPE matrix $\mathbf{M}_{HPE}$, that is, the two adaptations may use the same HPE matrix. Furthermore, Jiang et al.[37] gave an optimum solution to the yellow-blue and purple problems with the best matrix **M**, named as $\mathbf{M}_{OPT}$, achieving the following results: (a) using the matrix $\mathbf{M}_{OPT}$ the nesting rule is satisfied; (b) predicting the visual results,[21–33] the CIECAM02 model with the matrix $\mathbf{M}_{OPT}$ has better accuracy than the CIECAM02 model using any other matrix **M** satisfying the nesting rule. It was also found[37] that the CIECAM02 model with any of the matrices $\mathbf{M}_{02}$, $\mathbf{M}_{CAM}$, $\mathbf{M}_{HPE}$, and $\mathbf{M}_{OPT}$ has approximately the same accuracy in predicting the LUTCHI and Juan and Luo color appearance dataset.[21–27] The predictions of the corresponding color datasets[21,28–33] by the CAT02 transform (Equation 3) using different matrices were different however: specifically, the matrices $\mathbf{M}_{CAM}$, $\mathbf{M}_{HPE}$, and $\mathbf{M}_{OPT}$ provided worse results than the original matrix $\mathbf{M}_{02}$.

In 2008, Gill[17] also described an extension to the CIECAM02 model, where some of the equations were changed so that the modified version could avoid the mathematical failure of CIECAM02. Gill however, made no comparisons of predictions with visual data but the modified version should at least have the same accuracy in predicting the visual datasets as the original CIECAM02 model. The modified model was however, more complicated than the original.

All the above modifications to the CIECAM02 model lead to a model that has the same structure as the original model. Hence, the two adaptations are completed in different spaces. However, all the above modifications to the CIECAM02 model are either complicated or lose accuracy in predicting the corresponding color datasets. Specifically, the optimum solution found by Jiang et al.[37] is the best proposal we can achieve if we use the structure of the original CIECAM02 model. This induced us to consider that perhaps we must change the structure of the original CIECAM02 model to solve its problems and at the same time improve the accuracy of the predictions for the current corresponding color[21,28–33] and color appearance datasets.[21–27]

We now propose that the two adaptations, luminance, and color, be completed in the same space, and a new space be transformed from *X*, *Y*, and *Z* space via a new matrix, $\mathbf{M}_{16}$. As before, this matrix will be modelled as the optimum solution to a constrained nonlinear optimization problem to be solved numerically. The performance of a new CAT16 transform, (i.e., the old CAT02 transform with the new matrix $\mathbf{M}_{16}$), the CAM16 model (i.e., the new structure of the CIECAM02 model with the new matrix $\mathbf{M}_{16}$), and the CAM16-UCS uniform color space (i.e., the uniform color space based on the new CAM16 model) will be evaluated.

2 | THE NEW COLOR APPEARANCE MODEL

As discussed above, the new model completes the two adaptations in the same space, and the new matrix **M** maps the *X*, *Y*, and *Z* values to the new *R*, *G*, and *B* space. Firstly, one can imagine from Equations 3–7 that, if the same matrix **M** is used in lieu of both M_{02} and M_{HPE}, we have:

$$\begin{pmatrix} R' \\ G' \\ B' \end{pmatrix} = \begin{pmatrix} R_c \\ G_c \\ B_c \end{pmatrix} = \mathbf{\Lambda}(D)\mathbf{M} \begin{pmatrix} X \\ Y \\ Z \end{pmatrix}. \tag{11}$$

Hence, when the two adaptations are completed in the same space, the first benefit is that the new model is more simple than the original. Next, it follows from Equations 2, 5, 8, and 11 that, to let the achromatic signal *A* be non-negative, the response signals *R*, *G*, and *B* should be also non-negative, that is,

$$\begin{pmatrix} R \\ G \\ B \end{pmatrix} = \mathbf{M} \begin{pmatrix} X \\ Y \\ Z \end{pmatrix} \geq 0, \tag{12}$$

for both the 2° and 10° observers since the diagonal matrix $\mathbf{\Lambda}(D)$ (Equation 5) is always non-negative. In addition, the nesting rule (Equation 10) indicates that the matrix *M* must be chosen to satisfy Equation 13.

$$\Omega_{CIE} \subseteq \Omega_M \tag{13}$$

It can be further shown that these last two conditions (Equations 12 and 13) are satisfied by the constraint defined in Equation 14,

$$\begin{pmatrix} R \\ G \\ B \end{pmatrix} = \mathbf{M} \begin{pmatrix} \bar{x}(\lambda) \\ \bar{y}(\lambda) \\ \bar{z}(\lambda) \end{pmatrix} \geq 0, \tag{14}$$

where $\bar{x}(\lambda)$, $\bar{y}(\lambda)$, and $\bar{z}(\lambda)$ are the CIE (1931 or 1964) color-matching functions. Hence, if Equation 14 is satisfied, the achromatic signal A can be shown to be non-negative, resulting in proper values for the lightness J (Equation 1) since A_W is always positive.[11]

Let m_{ij} be the nine elements of the matrix M. Additional constraints set the sum of the elements of each row to be unity, that is,

$$\begin{pmatrix} 1 \\ 1 \\ 1 \end{pmatrix} = \mathbf{M} \begin{pmatrix} 1 \\ 1 \\ 1 \end{pmatrix} = \begin{pmatrix} m_{11}+m_{12}+m_{13} \\ m_{21}+m_{22}+m_{23} \\ m_{31}+m_{32}+m_{33} \end{pmatrix}. \tag{15}$$

Usually, the reference white stimulus can be matched by the mixture of one unit of all three primary colors in both the *RGB* and *XYZ* color systems.[39] These constraints were used for deriving the CAT02[1–3,12,16] and the CMCCAT2000[40] matrices. The HPE matrix[1–3] and the Bradford transform[28,41] also satisfy Equation 15.

Furthermore, for each matrix **M** satisfying Equations 14 and 15, we have a modified CAT02 transform and a modified CIECAM02 model. In other words, the modified CAT02 transform is the new matrix **M** replacing the CAT02 original matrix $\mathbf{M}_{02}$, while the modified CIECAM02 model is simply the new structure of the CIECAM02 model with the modified CAT02 transform rather than the original one.

Next, the matrix **M** was determined such that the modified CAT02 matrix best fits to the corresponding color datasets and the modified CIECAM02 model best fits to the LUTCHI color appearance datasets.

The corresponding color datasets used here[21,28–33] are the seven color datasets accumulated by Luo and Hunt.[22,41] Each dataset includes a number of corresponding colors defined by pairs of X, Y, and Z tristimulus values giving the same color appearance under two different illuminants, for example D65 and A. Altogether, these seven datasets provide 21 subsets and 584 pairs of corresponding colors and they provide the most reliable and comprehensive experimental data now available. They were used to derive the CAT02 matrix.[1–3,12,18] The weighted mean CIELAB color difference $\overline{\Delta E}$ between the predictions of the modified CAT02 transform and the experimental visual results was used here as a measure of the performance of the modified CAT02 matrix. The weighted mean was used because the more color pairs in a dataset, the larger weight it will contribute: the sum of all weights is equal to unity. It is clear that $\overline{\Delta E}$ depends on the elements of the matrix **M**, and hence $\overline{\Delta E}$ can be abbreviated as $\overline{\Delta E}(M)$.

The color appearance datasets are those accumulated at the Loughborough University of Technology Computer-Human Interface (LUTCHI) Research Centre[21–25] and those accumulated at the Color Imaging Institute of the University of Derby.[26,27] All these datasets were used to develop the CIECAM02 model[1,2] and to report on its performance.[3] The mean values of the Coefficient of Variation CV between the modified CIECAM02 model predictions of correlated color attributes (i.e., lightness, colorfulness, and hue composition) and the experimental visual results were used as a measure of the performance of the modified CIECAM02 model. Therefore, if P_i is the model prediction, and V_i the experimental visual result, the CV value[22] can be defined as:

$$\mathrm{CV} = 100 \sqrt{\frac{1}{n}\sum_{i=1}^{n}(P_i - V_i)^2} \Big/ \left(\frac{1}{n}\sum_{i=1}^{n} V_i\right). \tag{16}$$

where n is the number of samples in the dataset in question. If CV = 0, the agreement between the model predictions and the experimental visual results is perfect. If CV = 20, there is a 20% disagreement between the model predictions and the experimental visual results. The lower the CV value, the better the model performs. Let $\overline{\mathrm{CV}}$ be the mean CV value for all datasets considered here. Note that $\overline{\mathrm{CV}}$ is a function of the m_{ij} elements in matrix M, and hence it can be abbreviated to $\overline{\mathrm{CV}}(M)$. Note also that the CV value was used as a statistic during the development and evaluation of the earlier CIECAM97s model and the CIECAM02 model.[1–3]

From the above discussions, for final optimisation, an objective function $F(M)$ was defined as

$$F(M) = w_1 \overline{\Delta E}(M) + w_2 \overline{\mathrm{CV}}(M), \tag{17}$$

where both w_1 and w_2 were set equal to 0.5 to give the same load to visual results in corresponding color and color appearance datasets and also, because it was found that this combination of weights gave the best overall performance [i.e., the minimum value of the function $F(M)$].

The MATLAB routine *fmincon* was used to solve this constrained nonlinear optimization problem, considering the HPE matrix $\mathbf{M}_{HPE}$ as the initial guess. Finally, the matrix $\mathbf{M}_{16}$ was obtained numerically:

$$\mathbf{M}_{16} = \begin{pmatrix} 0.401288 & 0.650173 & -0.051461 \\ -0.250268 & 1.204414 & 0.045854 \\ -0.002079 & 0.048952 & 0.953127 \end{pmatrix}. \tag{18}$$

Thus, using $\mathbf{M}_{16}$ the two adaptations are made in only one new space and we have a new modified CAT02 transform (CAT16) and a new modified CIECAM02 model (CAM16). The full procedure for CAM16 is given in Appendix A.

In addition, the same equations used to extend the CIECAM02 model to include the CAM02-UCS color space[7]

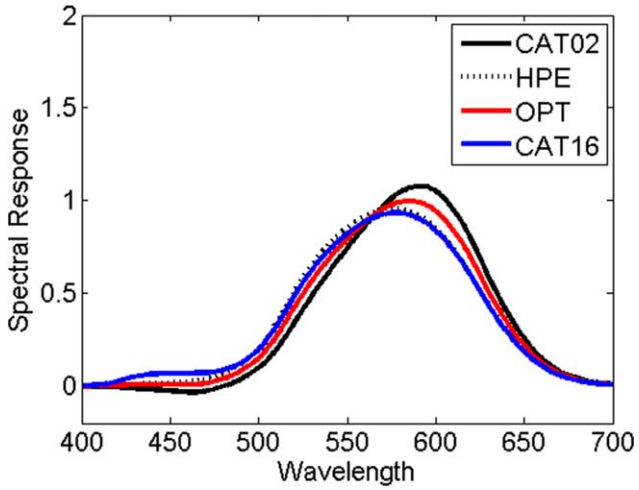

FIGURE 1 Spectral responses for the red channel with different matrices

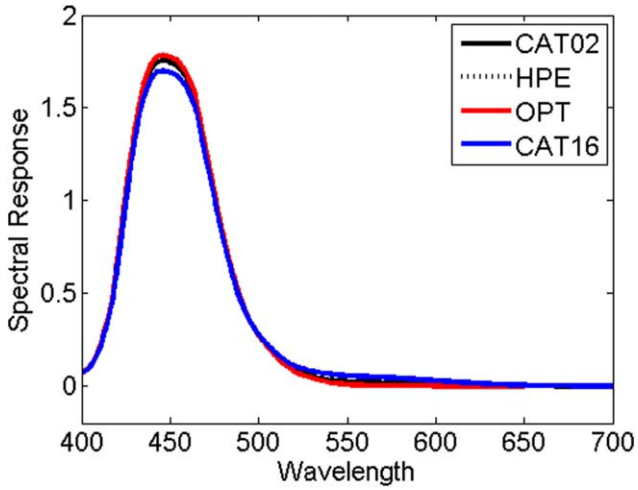

FIGURE 3 Spectral responses for the blue channel with different matrices

were also applied to the CAM16 model to produce the CAM16-UCS color space. In the next section, the performance of these new models, CAM16, CAT16, and CAM16-UCS, will be investigated.

3 | PERFORMANCE OF THE CAT16 TRANSFORM, THE CAM16 MODEL, AND THE CAM16-UCS COLOR SPACE

3.1 | Spectral responses

Spectral responses with each of the matrices $\mathbf{M}_{02}$, $\mathbf{M}_{HPE}$, $\mathbf{M}_{OPT}$, and $\mathbf{M}_{16}$ in the red, green and blue channels are plotted in Figures 1–3, respectively.

It can be seen from Figure 1 that, for the red spectral channel, the shapes are all similar, but the peaks are at slightly different positions. Specifically, relative to the peak position for the response of the matrix $\mathbf{M}_{OPT}$, the matrix $\mathbf{M}_{02}$ peaks toward a longer wavelength while the matrices $\mathbf{M}_{HPE}$ and $\mathbf{M}_{16}$ peak towards shorter wavelengths. We can also note that the matrix $\mathbf{M}_{02}$ has the highest/lowest spectral responses at long/short wavelengths. The spectral responses for the matrices $\mathbf{M}_{HPE}$ and $\mathbf{M}_{16}$ behave similarly but in opposite directions with respect to those of the matrix $\mathbf{M}_{02}$. The spectral response curve of the matrix $\mathbf{M}_{OPT}$ behaves in-between the two extreme responses in the visible range. In addition, all the responses were non-negative except at some wavelengths for the matrix M_{02}.

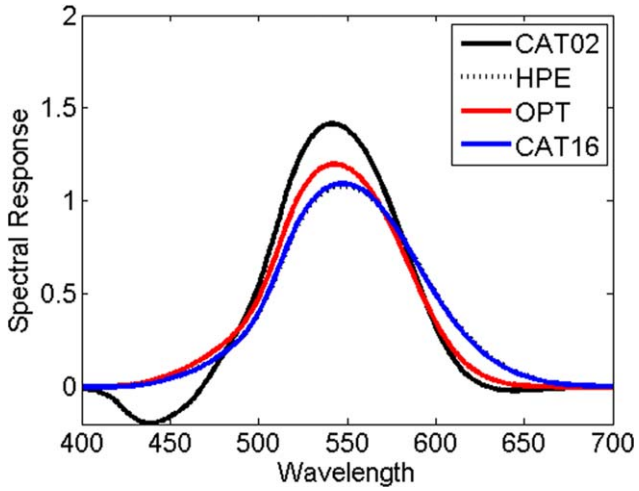

FIGURE 2 Spectral responses for the green channel with different matrices

For the green spectral channel, it can be seen from Figure 2 that all responses have one peak at approximately the same wavelength. However, the magnitudes of the responses are different, the highest being for $\mathbf{M}_{02}$, followed by $\mathbf{M}_{OPT}$, $\mathbf{M}_{16}$, and then M_{HPE}. The spectral responses of the matrices $\mathbf{M}_{16}$ and $\mathbf{M}_{HPE}$ are nearly identical. Again, the green channel response curves are always non-negative, except for the matrix $\mathbf{M}_{02}$.

Figure 3 shows that all blue response functions are similar, except around the peak at 450 nm and for wavelengths around 550 nm. The spectral responses of the matrices $\mathbf{M}_{OPT}$ and $\mathbf{M}_{HPE}$ were almost identical and they have the highest peak response, while the spectral response of the matrix M_{16} has the lowest peak response. All the spectral responses for the blue channel are non-negative.

Note that there is only one matrix, $\mathbf{M}_{02}$, for which the red and the green spectral responses had some negative values. Hence it has been widely agreed that the CAT02 adaptation should be carried out in a "sharp sensor" space.[42] However, the spectral responses for the matrix $\mathbf{M}_{HPE}$ are always non-negative, and therefore they are considered as cone-like responses.[14] Since the spectral responses for the matrix $\mathbf{M}_{16}$ (and the matrix $\mathbf{M}_{OPT}$) are similar to those of the matrix M_{HPE}, the spectral response space of the matrix $\mathbf{M}_{16}$

TABLE 1 The performance of various CATs in terms of CIELAB color difference units

Dataset	Reference Illuminant	Test Illuminant	No. of Sample Pairs	M_{02}	M_{HPE}	M_{OPT}	M_{16}
CSAJ	D65	A	87	4.0	5.5	5.0	4.3
Kuo	D65	A	40	5.0	6.8	6.1	5.8
Kuo	D65	TL84	41	3.5	4.9	4.7	3.8
Lam	D65	A	58	4.4	6.2	5.6	4.9
Helson	C	A	59	4.9	6.0	5.6	5.2
LUTCHI	D65	A	43	5.7	6.1	6.5	**5.6**
LUTCHI	D65	D50	44	6.6	**6.4**	**6.5**	6.6
LUTCHI	D65	WF	41	7.0	9.9	9.4	7.0
Breneman (1)	D65	A	12	7.7	8.0	**7.5**	7.7
Breneman (2)	D55	Projector	12	5.1	5.5	5.3	**4.7**
Breneman (3)	D55	Projector	12	8.2	11.1	10.9	**7.9**
Breneman (4)	D65	A	11	9.8	13.4	12.9	**9.6**
Breneman (6)	D65	A	12	7.5	**7.4**	7.6	**6.4**
Breneman (8)	D65	A	12	8.8	12.5	11.9	**8.7**
Breneman (9)	D65	A	12	14.2	18.9	18.4	**13.9**
Breneman (11)	Green	D55	12	6.6	**4.6**	**4.9**	**6.1**
Breneman(12)	Green	D55	12	7.2	**6.0**	**6.2**	**6.4**
Braun & Fairchild (1)	D65	D65	17	3.2	3.7	3.7	3.3
Braun & Fairchild (2)	D65	D65	16	5.1	5.3	5.3	**5.0**
Braun & Fairchild (3)	D65	D93	17	3.7	5.7	4.9	4.4
Braun & Fairchild (4)	D65	A	14	3.8	4.1	3.9	4.0
Overall Mean				6.3	7.5	7.3	6.3
Weighted Mean				5.5	6.8	6.5	5.6

Values in plain/(bold) font in the last three columns indicate where the original CAT02 transform is/(is not) better than the CAT02 transform with the corresponding matrices. The three values underlined indicate that the CAT02 and the CAT02 transform with the matrix $\mathbf{M}_{16}$ perform equally well.

can also be considered as a "cone-like" space. Thus, it can be concluded that adaptation using the CAT16 transform and the two adaptations of the CAM16 model were completed in a cone-like space.

3.2 | Predicting the corresponding color datasets

Four CATs with different matrices were tested: the CAT02 transform with the original matrix $\mathbf{M}_{02}$, plus three analogous transforms using the matrices $\mathbf{M}_{HPE}$, $\mathbf{M}_{OPT}$, and the new matrix $\mathbf{M}_{16}$, respectively. We have employed the available corresponding color datasets[21,28–33] used to derive the original matrix $\mathbf{M}_{02}$. Each corresponding color dataset includes a different number of sample pairs. Each pair includes two sets of X, Y, Z tristimulus values such that their corresponding appearances match under the reference and test illuminants. As mentioned before, the performance of each CAT02 transform has been measured using the mean values of CIELAB color differences between the X, Y, and Z values of the predicted corresponding colors and the experimental visual results. The smaller the value of mean color difference, the more accurately the transform performs. The results for each individual dataset are listed in Table 1, including the test and reference illuminants and the number of sample pairs. The last two rows in Table 1 show the overall mean and the

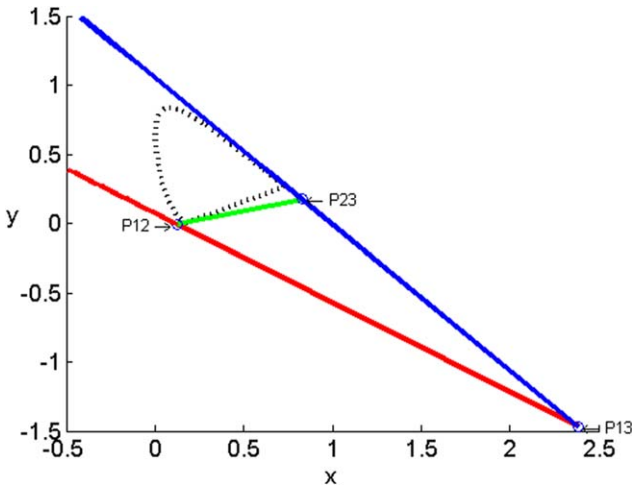

FIGURE 4 Triangle associated to the CAT16 matrix $\mathbf{M}_{16}$ in the CIE *x*,*y* chromaticity diagram.[37] The points P_{23}, $P_{13,}$ and P_{12} are the red, green, and blue primaries of the matrix, respectively. The dotted black line is the CIE spectrum locus and purple line. Thus, the region enclosed by the spectrum locus and the purple line is Ω_{CIE} in Equation 13. The non-negative response region Ω_M with $\mathbf{M}=\mathbf{M}_{16}$ for the CAT16 matrix is the open polygon, with one side open, which encloses Ω_{CIE}

weighted mean CIELAB color differences considering all the datasets. Note that in the last three columns of Table 1, the numbers in plain/bold format mean the CAT02 transform with corresponding matrices (indicated in the first row) perform worse/better than the original CAT02 transform for the respective datasets and the numbers underlined in the last column mean the CAT16 transform (the CAT02 transform with matrix $\mathbf{M}_{16}$) and the original CAT02 transform performs equally well for the datasets concerned.

It can be seen from Table 1 that the CAT02 transform with the original matrix $\mathbf{M}_{02}$ performed the best with an overall mean and weighted mean value of 6.3 and 5.5 CIELAB units, respectively. This was to be expected since the original matrix $\mathbf{M}_{02}$ was obtained by fitting these visual datasets.[12] The second best result is provided by the CAT02 transform with the matrix $\mathbf{M}_{16}$, that is, the proposed CAT16 transform, with an overall mean of 6.3 CIELAB units, identical to the value found for the original CAT02 transform, and a weighted mean value of 5.6 CIELAB units, which is only 0.1 CIELAB units higher than that found for the original CAT02 transform. Thus, it can be concluded that the CAT02 and CAT16 transforms perform equally well for these corresponding color datasets.[21,28–33] Table 1 also shows that the CAT02 transform with the matrix $\mathbf{M}_{OPT}$ ranks third. The worst case is the CAT02 transform with the matrix $\mathbf{M}_{HPE}$, which is perhaps understandable since, amongst the four matrices tested, only the matrix $\mathbf{M}_{HPE}$ was not derived by looking for a best fit of these visual datasets. However, when deriving the matrix $\mathbf{M}_{OPT}$ it was specifically intended to satisfy the nesting rule, not for deriving the matrix M_{16} (although the *de facto* positivity of the spectral curves of the $\mathbf{M}_{16}$ matrix implies that the chromaticity triangle of the $\mathbf{M}_{16}$ primaries contains the spectrum locus, as will be shown below. Another difference is that the structure of the CIECAM02 model was not changed when deriving the matrix $\mathbf{M}_{OPT}$, but this was not true when deriving the matrix $\mathbf{M}_{16}$. Hence, the structure of the model had an impact on the derivation of the matrix in the CAT02 transform.

Note that for the 21 individual datasets shown in Table 1, the original CAT02 transform performed better than the CAT02 transform with the HPE matrix $\mathbf{M}_{HPE}$ for 17 of those datasets. It can also be seen in Table 1 that the original CAT02 transform performed better than the CAT02 transform with the matrix $\mathbf{M}_{OPT}$ for 17 of the 21 datasets. However, almost equal performance was found for the original CAT02 and CAT16 transforms. Specifically, Table 1 shows that the original CAT02 transform performed better/worse than the CAT16 transform for 8/10 datasets, and these transforms perform equally well for 3 datasets. Thus, it can be concluded that the CAT16 and CAT02 transforms performed equally well.

3.3 | The nesting rule

We already know that the source of the problem in the CIECAM02 model is the original CAT02 matrix M_{02} which does not satisfy the nesting rule,[34–37] while the matrices $\mathbf{M}_{HPE}$ and $\mathbf{M}_{OPT}$ solve the problem and satisfy this rule: it is important that the matrix $\mathbf{M}_{16}$ should also satisfy the nesting rule. The structure of the CAM16 model is different from that of the original CIECAM02 model, and, under the new structure, the nesting rule is defined by Equation 13 with the matrix $\mathbf{M}$ set equal to the matrix $\mathbf{M}_{16}$. Figure 4 shows the red, green and blue primaries (P_{23}, $P_{13,}$ and P_{12}) associated with the matrix $\mathbf{M}_{16}$ in the CIE *x*,*y* chromaticity diagram, and the corresponding triangle.[37,38] In Figure 4, the red response *R* (see Equation 12) is equal to zero on the red line and greater than zero above the red line. Analogously, the green response *G* is equal to zero on the green line connecting the points P_{12} and P_{23} and positive above the green line. Finally, the blue response *B* is equal to zero on the blue line and positive below the blue line. Therefore, the positive response region Ω_M (with $\mathbf{M}=\mathbf{M}_{16}$) is the open "quadrilateral" region, which contains the domain Ω_{CIE} enclosed by the CIE spectrum locus and the purple line (the dotted black line). Hence, the nesting rule is satisfied.

3.4 | Performance of the CAM16 model when predicting the color appearance datasets

Using the LUTCHI color appearance datasets[21–25] and those data accumulated at the Color & Imaging Institute of the

TABLE 2 *CV* values for the lightness attribute in eight color appearance datasets considering the predictions made by the CIECAM02 model with three different CAT02 matrices (columns 2–4) and the CAM16 model (last column)

Group	M_{02}	M_{HPE}	M_{OPT}	M_{16}
RHL	10.6	10.9	10.9	10.7
RLL	11.4	11.7	11.6	11.5
RVL	13.3	13.5	13.5	13.3
RTE	14.8	14.8	14.8	14.8
CRT	11.6	11.7	11.7	11.6
M35	19.3	20.0	20.0	19.7
LTX	16.5	16.6	16.6	16.5
JUA	14.2	14.2	14.2	14.1
Mean	**14.0**	**14.2**	**14.2**	**14.0**

University of Derby,[26,27] we have tested the accuracy of four different color appearance models: the new CAM16 model (i.e., the new structure of the CIECAM02 model with the CAT16 transform given by the matrix $\mathbf{M}_{16}$), the original CIECAM02 model, and the CIECAM02 model with the matrices $\mathbf{M}_{HPE}$ and $\mathbf{M}_{OPT}$, respectively. For assessing the fit to the experimental data, we have employed the value of CV (Equation 16), already used to test the performance of previous color appearance models,[22] including CIECAM02.[3] The lower the CV value, the better the performance of the model.

Tables 2–4 show CV values for the appearance attributes lightness, colorfulness, and hue composition, respectively, considering each one of the four color appearance models tested and the eight appearance datasets. While Tables 2–4

TABLE 3 Idem to Table 2, but for the colorfulness attribute

Group	M_{02}	M_{HPE}	M_{OPT}	M_{16}
RHL	17.8	17.9	17.9	17.2
RLL	18.6	18.8	18.7	17.3
RVL	18.4	18.9	18.9	18.5
RTE	23.7	24.8	24.2	21.8
CRT	19.6	19.5	19.1	19.8
M35	16.1	16.2	16.2	16.9
LTX	14.2	14.4	14.4	15.1
JUA	20.3	20.2	20.3	19.3
Mean	**18.6**	**18.9**	**18.7**	**18.2**

TABLE 4 Idem to Table 2, but for the hue composition attribute

Group	M_{02}	M_{HPE}	M_{OPT}	M_{16}
RHL	6.9	6.9	6.8	6.4
RLL	7.1	7.2	7.0	6.7
RVL	6.5	6.5	6.5	6.7
RTE	7.1	7.1	6.9	6.9
CRT	6.7	7.6	7.4	6.6
M35	7.2	7.5	7.5	7.9
LTX	5.8	5.6	5.6	5.4
JUA	7.6	7.5	7.5	6.5
Mean	**6.9**	**7.0**	**6.9**	**6.6**

do not show big differences among the predictions from the four models, the CAM16 model performed at least as well as the CIECAM02 model for the lightness attribute (Table 2), and better than CIECAM02 model for the colorfulness (Table 3) and the hue composition (Table 4) attributes. Furthermore, Tables 2–4 show that the CAM16 and CIECAM02 models outperformed the remaining two models using the CIECAM02 structure with the $\mathbf{M}_{HPE}$ and $\mathbf{M}_{OPT}$ matrices.

3.5 | Predicting the color-difference datasets

To test the performance of different UCSs, the same three groups of color-difference datasets that were used to test the CAM02-UCS space[7] were used: small color differences (SCD), large color differences (LCD), and an illuminant A color-difference dataset (Table 5). The datasets in the first two groups were all obtained under daylight simulators, close to CIE illuminant D65. The SCD group has 3813 sample pairs with an average color difference of 2.0 CIELAB units and includes the four datasets most extensively studied in color-difference evaluation: RIT-DuPont,[43] Leeds,[44] BFD-P,[45] and Witt.[46] The LCD group has 2953 pairs with an average color difference of 11.1 CIELAB units and includes 6 datasets: OSA,[47] Munsell,[48,49] Attridge, and Pointer[50] (A & P), Guan,[51] Zhu,[52] and Badu-Textile.[53] The illuminant A group includes only one dataset,[54] BFDA, which was obtained under CIE illuminant A, having 1053 pairs of samples with an average color difference of 2.9 CIELAB units.

In 2006, Luo et al.[7] developed a uniform color space as an extension of the CIECAM02 color appearance model and made comprehensive comparisons with available UCSs and formulae using the three groups of datasets. It was found that the CAM02-UCS space performed well, and here, only the

TABLE 5 *STRESS* results for different color difference datasets[43–54] together with the mean values for the three groups SCD, LCD, and A

Group	Dataset	No. of pairs	Mean ΔE	CIECAM02	CAM02-UCS	CAM16	CAM16-UCS	CAM16-UCS with power correction
	RIT-DuPont	312	1.44	30.6	19.9	28.9	19.8	12.4
SCD	Leeds	307	1.63	40.0	25.3	38.7	24.5	20.8
	BFD	2776	3.00	39.0	31.1	38.8	30.9	30.8
	WITT	418	1.87	44.5	31.9	43.8	31.5	30.6
	Mean		2.00	38.5	27.1	37.6	26.7	23.6
	OSA	127	14.3	20.4	19.4	20.4	19.0	17.2
	Munsell	844	10.1	20.8	28.0	20.4	28.7	21.0
	A&P	1308	8.90	30.4	30.3	31	31.0	26.1
LCD	GUAN	292	11.4	25.6	18.6	24.8	17.2	13.1
	ZHU	144	9.9	27.3	25.9	28.2	26.7	16.6
	BADU-T	238	11.8	26.7	18.6	25.2	17.1	18.7
	Mean		11.1	25.2	23.5	25.0	23.3	18.8
A	BFDA	1053	2.9	37.7	31.3	35.2	29.9	25.9

Results under the power correction column were obtained with the power correction applied to the Euclidean color difference in CAM16-UCS space.

performance of the CIECAM02, CAM16, CAM02-UCS, and CAT16-UCS uniform color spaces are tested, and results presented in terms of the mean STRESS values[55] are listed in Table 5. The same equations as used in the CAM02-UCS space are used for extending CAM16 to derive the CAM16-UCS space. Furthermore, the power function:

$$\Delta E = 1.41\left(\Delta E'\right)^{0.63} \tag{19}$$

developed by Huang et al.[56] is applied to the color-difference metric associated with CAM16-UCS and the results are listed in the last column of Table 5. $\Delta E'$ is the color difference in terms of the J', $a_{M'}$, and $b_{M'}$ coordinates[7] in CAM16-UCS space.

The results in Table 5 show that for the SCD group, CAM16/CAM16-UCS are slightly better than CIECAM02/CAM02-UCS for each of the datasets in this group. For the LCD group, CIECAM02 performs better for two datasets, worse for three datasets and equally well for one the dataset. Overall, it can be said that CAM16 is slightly better than CIECAM02 for the LCD group. Comparing CAM02-UCS and CAM16-UCS in the LCD group, we note that CAM02-UCS performs better for three datasets and worse for three datasets, and overall CAM16-UCS is slightly better than CAM02-UCS by 0.2 *STRESS* units. Finally, for the illuminant A dataset, CAM16/CAM16-UCS performs better than CIECAM02/CAM02-UCS. These results are encouraging since the models CAM16/CAM16-UCS were not developed from these three groups of datasets. Overall, Table 5 shows that CAM16-UCS gave similar or better performance than CAM02-UCS. Therefore, it can be applied for all color-difference evaluation with confidence. Results in the last column of Table 5 also show that the color-difference metric associated with CAM16-UCS can be further improved by the use of the power correction function, Equation 19 proposed by Huang et al.[56]

3.6 | The use of the CAT16 CAT

It should be noted that, in the derivation of the CAT and in the methods used to obtain the corresponding color datasets listed in Table 1, the CAT always directly links a test illuminant to a reference illuminant. The reference illuminant is normally close to daylight (often illuminant D65). The (forward) CAT16 transform can in general be summarized as a one-step CAT defined by a 3 by 3 mapping matrix, $\mathbf{\Phi}_{r,t}$ given by:

$$\mathbf{\Phi}_{r,t} = \mathbf{M}_{16}^{-1}\mathbf{\Lambda}_{r,t}\mathbf{M}_{16} \tag{20}$$

where the subscripts r and t represent information under the reference and test illuminants, respectively. The diagonal adaptation matrix $\mathbf{\Lambda}_{r,t}$ is defined by

$$\mathbf{\Lambda}_{r,t}=\begin{pmatrix} D\cdot\frac{Y_w}{Y_{wr}}\cdot\frac{R_{wr}}{R_w}+1-D & 0 & 0 \\ 0 & D\cdot\frac{Y_w}{Y_{wr}}\cdot\frac{G_{wr}}{G_w}+1-D & 0 \\ 0 & 0 & D\cdot\frac{Y_w}{Y_{wr}}\cdot\frac{B_{wr}}{B_w}+1-D \end{pmatrix} \tag{21}$$

Which, when $Y_w=Y_{wr}=100$, reduces to $\Lambda(D)$ as given in Equation 5. The factor Y_w/Y_{wr} was first introduced by Li et al.[40] and its justification was given by Hunt et al.[57] Thus, the (forward) CAT16 or one-step CAT $\Phi_{r,t}$ maps the *X*, *Y*, and *Z* tristimulus values under the test illuminant to *X, Y*, and *Z* tristimulus values under the reference illuminant. The inverse of the CAT16 transform can also be defined by a 3 by 3 matrix, $\Psi_{t,r}$ defined by:

$$\mathbf{\Psi}_{t,r}=\mathbf{\Phi}_{r,t}^{-1}=(\mathbf{M}_{16}^{-1}\mathbf{\Lambda}_{r,t}\mathbf{M}_{16})^{-1}=\mathbf{M}_{16}^{-1}(\mathbf{\Lambda}_{r,t})^{-1}\mathbf{M}_{16} \tag{22}$$

Hence, $\mathbf{\Psi}_{t,r}$, the inverse of the CAT16 transform, maps the *X, Y*, and *Z* tristimulus values under the reference illuminant to the *X*, *Y*, and *Z* tristimulus values under the test illuminant. Proceeding with a direct transformation between reference and test illuminants can be called the one-step adaptation method.

Because of the form of Equation 20, the one-step method has the problem that a forward transformation from test to reference illuminant, followed by a forward transformation from reference to test illuminant, is not an identity transformation (except in certain special cases such as when $D = 1$), that is, the final transformed *X*, *Y*, and *Z* tristimulus values are not equal to the original input *X*, *Y*, and *Z* tristimulus values. More generally, the one-step method is not transitive: transformation from A to B, followed by transformation from B to C, is not the same as transformation from A to C.

An alternative two-step method does not have this problem. In the two-step method, a forward transformation from test *X*, *Y*, and *Z* values to an agreed-upon intermediate state (for example, the equal-energy illuminant, SE) can be performed followed by a reverse transformation from the intermediate state to the reference *X*, *Y*, and *Z* values. It can be shown that applying the two-step method from test to reference *X*, *Y*, and *Z* values, and then another two-step transformation from reference to test *X*, *Y*, and *Z* values (same formula, but with r and t interchanged) will produce an identity, as required. The more general transitivity property is also maintained by the two-step method.

Thus the procedure for the two step method is as follows. First, use $\mathbf{\Phi}_{se,t}$ to map the *X*, *Y*, *Z* values under the test illuminant to X_{se}, Y_{se}, Z_{se} under the intermediate equal-energy illuminant SE; then use $\mathbf{\Psi}_{r,se}$ to map X_{se}, Y_{se}, and Z_{se} to *X*, *Y*, and *Z* values under the reference illuminant. Thus, the CAT16 transform working in this manner can be considered as a two-step transform, which again can be defined by a 3 by 3 matrix $\mathbf{\Pi}_{r,t}$ and this matrix is the product of the matrix $\mathbf{\Psi}_{r,se}$ and the matrix $\mathbf{\Phi}_{se,t}$, that is

$$\begin{aligned}\mathbf{\Pi}_{r,t}&=\mathbf{\Psi}_{r,se}\cdot\mathbf{\Phi}_{se,t}\\&=\mathbf{M}_{16}^{-1}(\mathbf{\Lambda}_{se,r})^{-1}\mathbf{M}_{16}\cdot\mathbf{M}_{16}^{-1}\mathbf{\Lambda}_{se,t}\mathbf{M}_{16}\\&=M_{16}^{-1}(\Lambda_{se,r})^{-1}\Lambda_{se,t}M_{16}\end{aligned} \tag{23}$$

In addition, $\mathbf{\Pi}_{r,t}$ can also be defined by:

$$\begin{aligned}\mathbf{\Pi}_{r,t}&=\mathbf{\Phi}_{r,se}\cdot\mathbf{\Phi}_{se,t}\\&=\mathbf{M}_{16}^{-1}\mathbf{\Lambda}_{r,se}\mathbf{M}_{16}\cdot\mathbf{M}_{16}^{-1}\mathbf{\Lambda}_{se,t}\mathbf{M}_{16}\\&=\mathbf{M}_{16}^{-1}\mathbf{\Lambda}_{r,se}\mathbf{\Lambda}_{se,t}\mathbf{M}_{16}\end{aligned} \tag{24}$$

Two candidate methods that can be used to implement the CAT16 transform have been described in this article. An initial investigation has shown that the differences in predicting the visual datasets using the one-step and the two-step CATs are negligible and the results of this analysis will be described in a future paper.[58]

Finally, it should be emphasized that, up to now, in practical applications such as in predicting color inconstancy,[59,60] the shorter one-step method (as in the present article) has been widely used, and the consequences of the inconsistencies have been small. However, it might be better if we were to use the two-step CAT to achieve the transitive property and to be consistent with the CIECAM02 model.

4 | CONCLUSIONS

In this article, we first analyzed various methods to solve the problems of the CIECAM02 color appearance model, which led to the proposal of either the $\mathbf{M}_{HPE}$ or $\mathbf{M}_{OPT}$ matrices to replace the original CAT02 matrix, keeping the same structure as the original CIECAM02 model. It was subsequently found that both matrices failed because they focused on solving the mathematical problem in the CIECAM02 model at the expense of losing accuracy in the prediction of the results from visual experiments. We concluded that it was necessary to change the original CIECAM02 model structure. In this paper, the chromatic and luminance adaptations were combined to take place in a new "cone-like" space. A new matrix

M was found to satisfy the constraints set by Equations 14 and 15 and, at the same time, the new model accurately predicted the corresponding color and color-appearance datasets. This resulted in a new CAT named CAT16 and a new color appearance model named CAM16. Further evaluation showed that the CAT16 and CAT02 transforms performed equally well to predict the corresponding color datasets. Most importantly, the CAT16 matrix satisfies the nesting rule while the CAT02 matrix does not. When predicting the color appearance datasets, the CAM16 and CIECAM02 models performed equally well in predicting the lightness data, but the CAM16 model performed better than the CIECAM02 model in predicting the colorfulness and hue composition data. Furthermore, a new uniform color space, CAM16-UCS, was developed based on the CAM16 model. This space was tested using three groups of color-difference datasets, with small magnitude, large magnitude and illuminant A differences, respectively. The CAM16-UCS space predicts these color-difference datasets results at least equal to or better than the CAM02-UCS space. The CAM16-UCS color-difference formula can be further improved by a power correction to the Euclidean color difference.

In summary, according to our results, the CAM16/CAT16/CAM16-UCS model should be considered as a good candidate to replace the current CIECAM02/CAT02/CAM02-UCS model.

ACKNOWLEDGMENTS

Contract grant sponsors: National Natural Science Foundation of China (Grant numbers: 61178053, 61575090, 61475142); Ministry of Economy and Competitiveness of Spain (Research project FIS2016-80983-P), with contribution of European Regional Development Fund (ERDF); The Natural Science Foundation of Liaoning Province, China (Grant No. 2013020005).

REFERENCES

[1] CIE Publication 159:2004. A colour appearance model for colour management systems: CIECAM02. Vienna: CIE Central Bureau; 2004.

[2] Moroney N, Fairchild MD, Hunt RWG, Li CJ, Luo MR, Newman T. The CIECAM02 colour appearance models. In: Proceeding of Tenth Color Imaging Conference (CIC10); 2002; Scottsdale, AZ: IS&T. 23–27.

[3] Li CJ, Luo MR, Hunt RWG, Moroney N, Fairchild MD, Newman T. The performance of CIECAM02. In: Proceeding of Tenth Color Imaging Conference (CIC10); 2002; Scottsdale, Arizona. 28–32.

[4] Choi SY, Luo MR, Pointer MR, Rhodes PA. Investigation of large display color image appearance. I: Important factors affecting perceived quality. *J Imaging Sci Technol.* 2008;*52*:1–11.

[5] Choi SY, Luo MR, Pointer MR, Rhodes PA. Investigation of large display color image appearance. III: Modeling image naturalness. *J Imaging Sci Technol.* 2009;*53*:1–12.

[6] Li CJ, Luo MR, Cui GH. Colour-difference evaluation using colour appearance models. In: Proceeding of Eleventh Color Imaging Conference (CIC11); 2003; Scottsdale, AZ: IS&T. 127–131.

[7] Luo MR, Cui GH, Li CJ. Uniform colour spaces based on CIECAM02 colour appearance model. *Color Res Appl.* 2006;*31*:320–330.

[8] Tastl I, Bhachech M, Moroney N, Holm JICC. color management and CIECAM02. In Proceeding of Thirteenth Color Imaging Conference (CIC13); 2005; Scottsdale, AZ: IS&T. 217–223.

[9] Kuo C, Zeise E, Lai D. Robust CIECAM02 implementation and numerical experiment within an international color consortium workflow. *J Imaging Sci Technol.* 2008;*52*:61-

[10] Kuo C, Zeise E, Lai D. Robust CIECAM02 implementation and numerical experiment within an ICC workflow. In: Proceeding of Fourteenth Color Imaging Conference (CIC14); 2006; Scottsdale AZ: IS&T. 215–219.

[11] Li CJ, Luo MR. Testing the robustness of CIECAM02. *Color Res Appl.* 2005;*30*:99–106.

[12] Hunt RWG, Li CJ, Juan LY, Luo MR. Further improvements to CIECAM97s. *Color Res Appl.* 2002;*27*:164–170.

[13] Hunt RWG, Pointer MR. A colour appearance transform for the CIE 1931 standard colorimetric observer. *Color Res Appl.* 1985; *10*:165–179.

[14] Estévez O. On the fundamental data base of normal and dichromatic vision. PhD thesis, University of Amsterdam, The Netherlands, 1979.

[15] Hunt RWG, Li CJ, Luo MR. Dynamic cone response functions for models of colour appearance. *Color Res Appl.* 2003;*28*:82–88.

[16] Brill MH, Mahy M. Visualization of mathematical inconsistencies in CIECAM02. *Color Res Appl.* 2013;*38*:188–195.

[17] Gill GW. A solution to CIECAM02 numerical and range issues. The 16th Color and Imaging Conference; November 10-14, 2008; Portland, Oregon, USA. pp. 327–331.

[18] Luo MR, Li CJ. CIE color appearance models and associated color spaces. In: Schanda J, ed. *Colorimetry: Understanding the CIE System*. Chapter 11. Wiley, Hoboken, New Jersey, USA, 2007.

[19] Li CJ, Luo MR, Sun PL. A modification of CIECAM02 based on the Hunt Pointer Estevez matrix. *J Imaging Sci Technol.* 2013;*57*:1–8.

[20] Li CJ, Luo MR, Wang ZF. Different matrices for CIECAM02. *Color Res Appl.* 2014;*39*:143–153.

[21] Luo MR, Clarke AA, Rhodes PA, Schappo A, Scrivener SAR, Tait CJ. Quantifying colour appearance. Part I. LUTCHI colour appearance data. *Color Res Appl.* 1991;*16*:166–180.

[22] Luo MR, Hunt RWG. Testing colour appearance models using corresponding-colour and magnitude-estimation data sets. *Color Res Appl.* 1998;*23*:147–153.

[23] Luo MR, Clarke AA, Rhodes PA, Schappo A, Scrivener SAR, Tait CJ. Quantifying colour appearance. Part II. Testing colour models performance using LUTCHI colour appearance data. *Color Res Appl.* 1991;*16*:181–197.

[24] Luo MR, Gao XW, Rhodes PA, Xin HJ, Clarke AA, Scrivener SAR. Quantifying colour appearance. Part III. Supplementary LUTCHI colour appearance data. *Color Res Appl.* 1993;*18*:98–113.

[25] Luo MR, Gao XW, Rhodes PA, Xin HJ, Clarke AA, Scrivener SAR. Quantifying colour appearance. Part IV. Transmissive media. *Color Res Appl.* 1993;*18*:191–209.

[26] Juan LG, Luo MR. *New Magnitude Estimation Data for Evaluating Colour Appearance Models. Colour and Visual Scales 2000, NPL.* Royal Holloway College, University of London, Egham, UK; 3-5 April, 2000.

[27] Juan LG, Luo MR. Magnitude estimation for scaling saturation. In: Proceeding of 9th Congress of the International Colour Association (AIC 2001). vol 4421. Rochester, USA: SPIE; 2002: 575–578.

[28] Lam KM. Metamerism and colour constancy. PhD thesis, University of Bradford, UK; 1985.

[29] Mori L, Sobagaki H, Komatsubara H, Ikeda K. Field trials on CIE chromatic adaptation formula. In: *Proceeding of CIE 22nd Session;* Melbourne, Australia, 1991:55–58.

[30] Kuo WG, Luo MR, Bez HE. Various chromatic-adaptation transformations tested using new colour appearance data in textiles. *Color Res Appl.* 1995;*20*:313–327.

[31] Helson H, Judd DB, Warren MH. Object-color changes from daylight to incandescent filament illumination. *Illum Eng.* 1952; *47*:221–233.

[32] Breneman EJ. Corresponding chromaticities for different states of adaptation to complex visual fields. *J Opt Soc Am A.* 1987;*4*: 1115–1129.

[33] Braun KM, Fairchild MD. Psychophysical generation of matching images for cross-media colour reproduction. In: Proceeding of Fourth Color Imaging Conference (CIC4); Scottsdale AZ: IS&T; 1996:214–220.

[34] Brill MH. Irregularity in CIECAM02 and its avoidance. *Color Res Appl.* 2006;*31*:142–145.

[35] Süsstrunk S, Brill MH. The nesting instinct: Repairing non-nested gamuts in CIECAM02. Late-breaking-news paper at Fourteenth Color Imaging Conference (CIC14), Scottsdale AZ; 2006.

[36] Brill MH, Süsstrunk S. Repairing gamut problems in CIECAM02: A progress report. *Color Res Appl.* 2008;*33*:424–426.

[37] Jiang J, Wang Z, Luo MR, Melgosa M, Brill MH, Li C. Optimum solution of the CIECAM02 yellow-blue and purple problems. *Color Res Appl.* 2015;*40*:491–503.

[38] Li CJ, Ji CJ, Luo MR, Melgosa M, Brill MH. CAT02 and HPE triangles. *Color ResAppl.* 2015;*40*:30–39.

[39] Ohta N, Robertson AR. *Colorimetry: Fundamentals and Applications*. Wiley, Chichester, England, 2005.

[40] Li CJ, Luo MR, Rigg B, Hunt RWG. CMC 2000 chromatic adaptation transform: CMCCAT2000. *Color Res Appl.* 2002;*27*: 49–58.

[41] Luo MR, Hunt RWG. A chromatic adaptation transform and a colour inconstancy index. *Color Res Appl.* 1998;*23*:154–158.

[42] Finlayson GD, Susstrunk S. Spectral sharpening and the Bradford transform. In: *Proceeding of Eighth IS&T/SID Colour Image Science.* Scottsdale, Arizona, USA, 2000;49–55.

[43] Berns RS, Alman DH, Reniff L, Snyder GD, Balonon-Rosen MR. Visual determination of suprathreshold color-difference tolerances using probit analysis. *Color Res Appl.* 1997;*16*:297–316.

[44] Kim DH, Nobbs J. New weighting functions for weighted CIELAB color difference formula. *Proc AIC Colour.* 1997;*1*: 446–449.

[45] Luo MR, Rigg B. Chromaticity-discrimination ellipses for surface colors. *Color Res Appl.* 1986;*11*:25–42.

[46] Witt K. Geometric relations between scales of small colour differences. *Color Res Appl.* 1999;*24*:78–92.

[47] MacAdam DL. Uniform color scales. *J Opt Soc Am.* 1974;*64*: 1691–1702.

[48] Newhall SM. Preliminary report of the O.S.A. subcommittee on the spacing of the Munsell colors. *J Opt Soc Am.* 1940;*30*:617–645.

[49] Newhall SM, Nickerson D, Judd DB. Final report of the O.S.A. subcommittee on the spacing of the Munsell colors. *J Opt Soc Am.* 1943;*33*:385–411.

[50] Pointer MR, Attridge GG. Some aspects of the visual scaling of large color differences. *Color Res Appl.* 1997;*22*:298–307.

[51] Guan S-S, Luo MR. A colour-difference formula for assessing large colour differences. *Color Res Appl.* 1999;*24*:344–355.

[52] Zhu SY, Luo MR, Cui G. New experimental data for investigating uniform colour spaces. *Proc AIC Color.* 2001;626–629.

[53] Badu AS. Large colour differences between surface colours. PhD thesis, University of Bradford, UK, 1986.

[54] Luo MR, Rigg B. A colour difference formula for surface colours under illuminant A. *J Soc Dyers Col.* 1987;*103*:161–167.

[55] García PA, Huertas R, Melgosa M, Cui G. Measurement of the relationship between perceived and computed color differences. *J Opt Soc Am A.* 2007;*24*:1823–1829.

[56] Huang M, Cui G, Melgosa M, et al. Power functions improving the performance of color-difference formulas. *Opt. Express.* 2015;*23*(1):597–610.

[57] Hunt RWG, Li CJ, Luo MR. Chromatic Adaptation Transforms. *Color Res Appl.* 2005;*30*:69–71.

[58] Li CJ, Wang Z, Xu Y, et al. Various possible usages of the CAT16 and their performance in predicting visual datasets, in preparation.

[59] ISO 105-J05. Textiles – Test of textile fastness – Part J05: Method for the instrumental assessment of colour inconstancy of a specimen with change in illuminant (CMCCON02). Geneva: International Organization for Standardardization; 2007.

[60] Luo MR, Li CJ, Hunt RWG, Rigg B. The CMC 2002 Colour Inconstancy Index: CMCCON02. J *Coloration Technol.* 2003; *119*:280–285.

How to cite this article: Li C, Li Z, Wang Z, et al. Comprehensive color solutions: CAM16, CAT16, and CAM16-UCS. *Color Res Appl.* 2017;42:703–718. https://doi.org/10.1002/col.22131

APPENDIX A
COLOR APPEARANCE MODEL CAM16

Part 1: Forward CAM16 model

Input: X, Y, Z (under test illuminant X_w, Y_w, and Z_w)

Output: Correlates of lightness J, chroma C, hue composition H, hue angle h, colorfulness M, saturation s, and brightness Q

Illuminants, viewing surrounds set up and background parameters

(See the note at the end of Part 2 of Appendix B for determining all parameters)

Adopted white in test illuminant: X_w, Y_w, Z_w

Background in test conditions: Y_b

Reference white in reference illuminant: $X_{wr} = Y_{wr} = Z_{wr} = 100$, fixed in the model

Luminance of test adapting field (cd/m^2): L_A

Surround parameters are given in next Table A1:

To determine the surround conditions see the note at the end of Part 1 of Appendix A.

N_c and F are modelled as a function of c, and their values can be linearly interpolated (see Figure A1), using the above points

Step 0: Calculate all values/parameters which are independent of the input sample

$$\begin{pmatrix} R_w \\ G_w \\ B_w \end{pmatrix} = \mathbf{M}_{16} \cdot \begin{pmatrix} X_w \\ Y_w \\ Z_w \end{pmatrix}, D = F \cdot \left[1 - \left(\frac{1}{3.6}\right) \cdot e^{\left(\frac{-L_A-42}{92}\right)}\right]$$

If D is greater than one or less than zero, set it to one or zero, respectively.

$$D_R = D \cdot \frac{Y_w}{R_w} + 1 - D, \quad D_G = D \cdot \frac{Y_w}{G_w} + 1 - D, \quad D_B = D \cdot \frac{Y_w}{B_w} + 1 - D,$$

$$F_L = 0.2\,k^4\,(5\,L_A) + 0.1\,(1-k^4)^2\,(5\,L_A)^{1/3},$$

where $k = \frac{1}{5 \cdot L_A + 1}$.

$$n = \frac{Y_b}{Y_w}, \quad z = 1.48 + \sqrt{n}, \quad N_{bb} = 0.725 \cdot \left(\frac{1}{n}\right)^{0.2}, \quad N_{cb} = N_{bb}$$

TABLE A1 Surround parameters

	F	c	N_c
Average	1.0	0.69	1.0
Dim	0.9	0.59	0.9
Dark	0.8	0.525	0.8

$$\begin{pmatrix} R_{wc} \\ G_{wc} \\ B_{wc} \end{pmatrix} = \begin{pmatrix} D_R \cdot R_w \\ D_G \cdot G_w \\ D_B \cdot B_w \end{pmatrix},$$

$$R_{aw} = 400 \cdot \left(\frac{\left(\frac{F_L \cdot R_{wc}}{100}\right)^{0.42}}{\left(\frac{F_L \cdot R_{wc}}{100}\right)^{0.42} + 27.13} \right) + 0.1$$

$$G_{aw} = 400 \cdot \left(\frac{\left(\frac{F_L \cdot G_{wc}}{100}\right)^{0.42}}{\left(\frac{F_L \cdot G_{wc}}{100}\right)^{0.42} + 27.13} \right) + 0.1$$

$$B_{aw} = 400 \cdot \left(\frac{\left(\frac{F_L \cdot B_{wc}}{100}\right)^{0.42}}{\left(\frac{F_L \cdot B_{wc}}{100}\right)^{0.42} + 27.13} \right) + 0.1$$

$$A_w = [2 \cdot R_{aw} + G_{aw} + \frac{B_{aw}}{20} - 0.305] \cdot N_{bb}$$

Note that all parameters computed in this step are needed for the following calculations. However, because they depend only on surround and viewing conditions, when processing pixels of an image they are computed only once. The next computing steps are sample (pixel) dependant.

Step 1: Calculate 'cone' responses

$$\begin{pmatrix} R \\ G \\ B \end{pmatrix} = \mathbf{M}_{16} \cdot \begin{pmatrix} X \\ Y \\ Z \end{pmatrix}$$

Step 2: Complete the color adaptation of the illuminant in the corresponding cone response space (considering various luminance levels and surround conditions included in D, and hence in D_R, D_G, and D_B)

$$\begin{pmatrix} R_c \\ G_c \\ B_c \end{pmatrix} = \begin{pmatrix} D_R \cdot R \\ D_G \cdot G \\ D_B \cdot B \end{pmatrix}$$

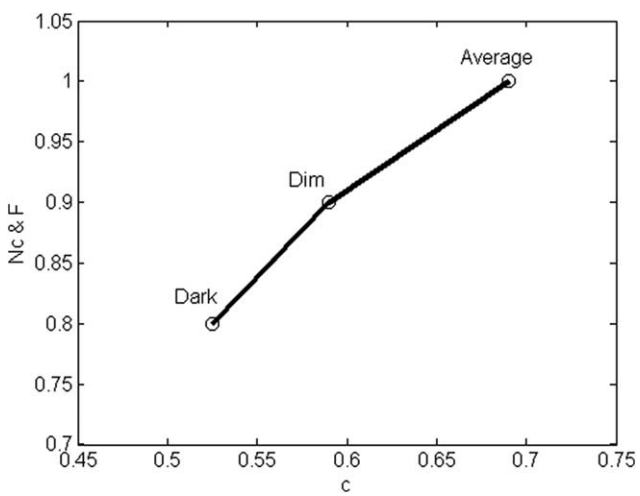

FIGURE A1 Linear interpolation to obtain N_c and F

TABLE A2 Unique hue data for calculation of hue quadrature

	Red	Yellow	Green	Blue	Red
i	1	2	3	4	5
h_i	20.14	90.00	164.25	237.53	380.14
e_i	0.8	0.7	1.0	1.2	0.8
H_i	0.0	100.0	200.0	300.0	400.0

Step 3: Calculate the postadaptation cone response (resulting in dynamic range compression)

$$R_a = 400 \cdot \left(\frac{\left(\frac{F_L \cdot R_c}{100}\right)^{0.42}}{\left(\frac{F_L \cdot R_c}{100}\right)^{0.42} + 27.13} \right) + 0.1$$

If R_c is negative, then

$$R_a = -400 \cdot \left(\frac{\left(\frac{-F_L \cdot R_c}{100}\right)^{0.42}}{\left(\frac{-F_L \cdot R_c}{100}\right)^{0.42} + 27.13} \right) + 0.1,$$

and similarly for the computations of G_a and B_a.

Step 4: Calculate Redness – Greenness (a), Yellowness – Blueness (b) components, and hue angle (h):

$$a = R_a - \frac{12 \cdot G_a}{11} + \frac{B_a}{11}$$

$$b = \frac{(R_a + G_a - 2 \cdot B_a)}{9}$$

$$h = \tan^{-1}\left(\frac{b}{a}\right)$$

(make sure h is between 0° and 360°)

Step 5: Calculate eccentricity [e_t, hue quadrature composition (H) and hue composition (H_c)]

Using the following unique hue data in Table A2, set $h' = h + 360$ if $h < h_1$, otherwise $h' = h$. Choose a proper i (i=1,2,3, or 4) so that $h_i \le h' < h_{i+1}$. Calculate

$$e_t = \frac{1}{4} \cdot \left[\cos\left(\frac{h' \cdot \pi}{180} + 2 \right) + 3.8 \right]$$

which is close to, but not exactly the same as, the eccentricity factor given in Table A2.

Hue Quadrature H is computed using the formula:

$$H = H_i + \frac{100 \cdot \frac{h' - h_i}{e_i}}{\frac{h' - h_i}{e_i} + \frac{h_{i+1} - h'}{e_{i+1}}}$$

and hue composition H_c is computed according to H. If $i = 3$ and $H = 241.2116$ for example, then H is between H_3 and H_4 (see Table A2 above). Compute $P_L = H_4 - H = 58.7884$; $P_R = H - H_3 = 41.2116$ and round P_L and P_R values to integers 59 and 41. Thus, according to Table A2, this sample is considered as having 59% of Green and 41% of Blue, which is the Hc and can be reported as 59G41B or 41B59G.

Step 6: Calculate achromatic response A

$$A = [2 \cdot R_a + G_a + \frac{B_a}{20} - 0.305] \cdot N_{bb}$$

Step 7: Calculate the correlate of lightness J

$$J = 100 \cdot \left(\frac{A}{A_w}\right)^{c \cdot z}$$

Step 8: Calculate the correlate of brightness Q

$$Q = \left(\frac{4}{c}\right) \cdot \left(\frac{J}{100}\right)^{0.5} \cdot (A_w + 4) \cdot F_L^{0.25}$$

Step 9: Calculate the correlates of chroma (C), colorfulness (M), and saturation (s)

$$t = \frac{\left(\frac{50{,}000}{13} \cdot N_c \cdot N_{cb}\right) \cdot e_t \cdot (a^2 + b^2)^{1/2}}{R_a + G_a + \left(\frac{21}{20}\right) \cdot B_a}$$

$$C = t^{0.9} \cdot \left(\frac{J}{100}\right)^{0.5} \cdot (1.64 - 0.29^n)^{0.73}$$

$$M = C \cdot F_L^{0.25}$$

$$s = 100 \cdot \left(\frac{M}{Q}\right)^{0.5}$$

Part 2: The Inverse CAM16 model.

Input: J or Q; C, M, or s; H or h

Output: X, Y, Z (under test illuminant X_w, Y_w, Z_w)

Illuminants, viewing surrounds, and background parameters are the same as those given in the forward model. See notes at the end of Part 2 of current Appendix A for calculating/defining the luminance of the adapting field and surround conditions.

Step 0: Calculate viewing parameters

Compute F_L, n, z, $N_{bb} = N_{bc}$, R_w, G_w, B_w, D, D_R, D_G, D_B, R_{wc}, G_{wc}, B_{wc}, R_{aw}, G_{aw}, B_{aw}, and A_w using the same formulae in Step 0 of the Forward model. Note that all data computed in this step can be used for all samples (for example all pixels in an image) under the viewing conditions. Hence, they are computed only once. The following computing steps are sample dependent.

Step 1: Obtain J, C, and h from H, Q, M, s

The input data can be different combinations of perceived correlates, that is, J or Q; C, M, or s; and H or h. Hence the following sub-steps are needed to convert the input parameters to the parameters J, C, and h.

Step 1-1: Compute J from Q (if input is Q)

$$J = 6.25 \cdot \left[\frac{c \cdot Q}{(A_w + 4) \cdot F_L^{0.25}}\right]^2$$

Step 1-2: Calculate C from M or s

$$C=\frac{M}{F_{\mathrm{L}}^{0.25}}(\text{if input is } M)$$

$$Q=\left(\frac{4}{c}\right)\cdot\left(\frac{\mathrm{J}}{100}\right)^{0.5}\cdot(A_{\mathrm{w}}+4.0)\cdot F_{\mathrm{L}}^{0.25}$$

and $C=(\frac{s}{100})^2\cdot(\frac{Q}{F_{\mathrm{L}}^{0.25}})$ (if input is s)

Step 1-3: Calculate h from H (if input is H)

The correlate of hue (h) can be computed by using data in Table A2 in the Forward model.

Choose a proper i (i =1, 2, 3, or 4) so that $H_i \le H < H_{i+1}$.

$$h'=\frac{(H-H_i)\cdot(e_{i+1}h_i-e_i\cdot h_{i+1})-100\cdot h_i\cdot e_{i+1}}{(H-H_i)\cdot(e_{i+1}-e_i)-100\cdot e_{i+1}}$$

Set $h=h'-360$ if $h' > 360$, otherwise $h=h'$.

Step 2: Calculate t, e_t, A, p_1, p_2, and p_3

$$t=\left[\frac{C}{\sqrt{\frac{J}{100}}\cdot(1.64-0.29^n)^{0.73}}\right]^{\frac{1}{0.9}}$$

$$e_t=\frac{1}{4}\cdot\left[\cos\left(h\cdot\frac{\pi}{180}+2\right)+3.8\right]$$

$$A=A_{\mathrm{w}}\cdot\left(\frac{J}{100}\right)^{\frac{1}{c\cdot z}}$$

$$p_1=\left(\frac{50,000}{13}\cdot N_{\mathrm{c}}\cdot N_{\mathrm{cb}}\right)\cdot e_t\cdot\left(\frac{1}{t}\right),\qquad \text{if}\quad t\neq 0$$

$$p_2=\frac{A}{N_{\mathrm{bb}}}+0.305$$

$$p_3=\frac{21}{20}$$

Step 3: Calculate a and b

If $t=0$, then $a=b=0$ and go to Step 4

In next computations be transform h from degrees to radians before calculating sin (h) and cos (h):

If $|\sin(h)| \ge |\cos(\mathrm{h})|$ then

$$p_4=\frac{p_1}{\sin(h)}$$

$$b=\frac{p_2\cdot(2+p_3)\cdot\left(\frac{460}{1403}\right)}{p_4+(2+p_3)\cdot\left(\frac{220}{1403}\right)\cdot\left(\frac{\cos(h)}{\sin(h)}\right)-\left(\frac{27}{1403}\right)+p_3\cdot\left(\frac{6300}{1403}\right)}$$

$$a=b\cdot\left(\frac{\cos(h)}{\sin(h)}\right)$$

If $|\cos(h)|>|\sin(\mathrm{h})|$, then

$$p_5=\frac{p_1}{\cos(h)}$$

$$a=\frac{p_2\cdot(2+p_3)\cdot\left(\frac{460}{1403}\right)}{p_5+(2+p_3)\cdot\left(\frac{220}{1403}\right)-\left[\left(\frac{27}{1403}\right)-p_3\cdot\left(\frac{6300}{1403}\right)\right]\cdot\left(\frac{\sin(h)}{\cos(h)}\right)}$$

$$b=a\cdot\left(\frac{\sin(h)}{\cos(h)}\right)$$

Step 4: Calculate R_a, G_a, and B_a

$$R_{\mathrm{a}}=\frac{460}{1403}\cdot p_2+\frac{451}{1403}\cdot a+\frac{288}{1403}\cdot b$$

$$G_{\mathrm{a}}=\frac{460}{1403}\cdot p_2-\frac{891}{1403}\cdot a-\frac{261}{1403}\cdot b$$

$$B_{\mathrm{a}}=\frac{460}{1403}\cdot p_2-\frac{220}{1403}\cdot a-\frac{6300}{1403}\cdot b$$

Step 5: Calculate R_{c}, G_{c}, and B_{c}

$$R_{\mathrm{c}}=\mathrm{sign}(R_{\mathrm{a}}-0.1)\cdot\frac{100}{F_{\mathrm{L}}}\cdot\left[\frac{27.13\cdot|R_{\mathrm{a}}-0.1|}{400-|R_{\mathrm{a}}-0.1|}\right]^{\frac{1}{0.42}}$$

$$\text{Here, } \mathrm{sign}(x)=\begin{cases}1 & \text{if} \quad x>0\\ 0 & \text{if} \quad x=0\\ -1 & \text{if} \quad x<0\end{cases}, \text{ and similarly}$$

computing G_{c}, and B_{c} from G_{a}, and B_{a}.

Step 6: Calculate R, G, and B from R_{c}, G_{c}, and B_{c}

$$\begin{pmatrix}R\\G\\B\end{pmatrix}=\begin{pmatrix}\frac{R_{\mathrm{c}}}{D_{\mathrm{R}}}\\ \frac{G_{\mathrm{c}}}{D_{\mathrm{G}}}\\ \frac{B_{\mathrm{c}}}{D_{\mathrm{B}}}\end{pmatrix}$$

Step 7: Calculate X, Y, and Z (for the coefficients of the inverse matrix, see the note at the end of the appendix B)

$$\begin{pmatrix}X\\Y\\Z\end{pmatrix}=M_{16}^{-1}\cdot\begin{pmatrix}R\\G\\B\end{pmatrix}$$

Notes to Appendices A

1. It is recommended to use the matrix coefficients given below for the inverse matrix

$$M_{16}^{-1}=\begin{pmatrix}1.86206786 & -1.01125463 & 0.14918677\\ 0.38752654 & 0.62144744 & -0.00897398\\ -0.01584150 & -0.03412294 & 1.04996444\end{pmatrix}$$

2. The L_{A} is computed using Equation A1

$$L_{\mathrm{A}}=\left(\frac{E_{\mathrm{W}}}{\pi}\right)\cdot\left(\frac{Y_{\mathrm{b}}}{Y_{\mathrm{W}}}\right)=\frac{L_{\mathrm{W}}\cdot Y_{\mathrm{b}}}{Y_{\mathrm{W}}},\qquad (\mathrm{A1})$$

where $E_{\mathrm{w}}=\pi L_{\mathrm{w}}$ is the illuminance of reference white in lux; L_{w} is the luminance of reference white in cd/m^2, Y_{b} is the luminance factor of the background, and Y_{w} is the luminance factor of the reference white.

3. Surround conditions (average, dim, and dark) are determined by the surround ratio S_R given by Equation A2:

$$S_R = \frac{L_{SW}}{L_{DW}} \tag{A2}$$

where L_{SW} is the luminance of the reference white measured in the surround field and L_{DW} is the luminance of the reference white measured in the display area. If S_R is 0, then the surround condition is "dark"; if $0 < S_R < 0.2$, then the surround is "dim"; and if $S_R \geq 0.2$, then the surround is "average."

APPENDIX B
UNIFORM COLOR SPACE: CAM16-UCS

Let the J, M, and h be lightness, colorfulness, and hue angle, respectively, computed using the CAM16 model. The UCS based on CAM16 is given by next Equations:

$$\begin{aligned} J' &= \frac{1.7J}{1+0.007J} \\ M' &= \ln(1+0.0228M)/0.0228 \\ a' &= M'\cos(h) \\ b' &= M'\sin(h) \\ h' &= h \end{aligned} \tag{A3}$$

The J', a', and b' coordinates define the approximately uniformity color space associated to the CAM16 model, shortened as CAM16-UCS. The color difference between two samples can be computed as the Euclidean distance between them in CAM16-UCS:

$$\Delta E' = \sqrt{\Delta J'2 + \Delta a'2 + \Delta b'2} \tag{A4}$$

where the $\Delta J'$, $\Delta a'$, and $\Delta b'$ are the J', a', and b' differences between the pair of samples, respectively.

$$\Delta E = 1.41\left(\Delta E'\right)^{0.63} \tag{A5}$$